*Article*

# The Lyavaraka Ultrabasic Complex, Serpentinite Belt, Kola Peninsula, Russia

Andrei Y. Barkov [1], Andrey A. Nikiforov [1], Vladimir N. Korolyuk [2] and Robert F. Martin [3],*

[1] Research Laboratory of Industrial and Ore Mineralogy, Cherepovets State University, 5 Lunacharsky Avenue, 162600 Cherepovets, Russia
[2] V.S. Sobolev Institute of Geology and Mineralogy, Siberian Branch of the Russian Academy of Science, 3 Avenue "Prospekt Koptyuga", 630090 Novosibirsk, Russia
[3] Department of Earth and Planetary Sciences, McGill University, 3450 University Street, Montreal, QC H3A 0E8, Canada
* Correspondence: robert.martin@mcgill.ca

**Abstract:** The Paleoproterozoic Lyavaraka ultrabasic complex is one of several dunite–harzburgite–orthopyroxenite bodies exposed as shallow plutonic complexes in the Serpentinite Belt, Kola Peninsula, Russia. Lyavaraka and the other complexes are anorogenic, formed in a stable within-plate environment in the interval 2.5–2.4 Ga as members of a large igneous province formed in the Sumian cycle of igneous activity. This geotectonic setting accounts for the shallow emplacement of the strongly magnesian komatiitic magma in the Fennoscandian Shield. We recognize three stages of crystallization of the Al-undepleted magma, present as dislocated blocks. Zone I is the ultrabasic core-like zone in which olivine predominates. Orthopyroxene is the major mineral in Zone II, and Zone III contains the most evolved ultrabasic rocks in which recurrent olivine coexists with Cpx + Pl. Primocrysts of hypermagnesian Opx (Mg# 91–93) nucleated in central areas of Zone II as olivine (Mg# 89.1–90.3) was forming in Zone I. In Zone III, olivine grains of a second generation (Mg# 74.5–75.8) formed after the primocrystic Cpx (Mg# up to 88.0) appeared. The recurrence of olivine is attributed to the progressive buildup in $f$O$_2$ as a result of degassing and conversion of Fe$^{2+}$ to Fe$^{3+}$, well documented in our earlier studies of oxide parageneses.

**Keywords:** Lyavaraka complex; dunite–harzburgite–orthopyroxenite association; komatiitic magma; highly magnesian melt; degassing; progressive oxidation; Serpentinite Belt; Kola Peninsula; Russia

## 1. Introduction

The Serpentinite Belt [1–3] consists of the Paleoproterozoic Pados-Tundra layered complex [4–10] and accompanying suites of ultrabasic shallow plutonic and subvolcanic rocks. The belt extends for over two hundred kilometers in the Kola Peninsula and continues westward as the Tulppio Belt in Finland [11]. The Serpentinite Belt includes the large zoned sills of the Chapesvara complex and the differentiated Khanlauta flow [12,13]. The emplacement of these highly magnesian complexes likely proceeded in response to a large-scale mantle plume of rising komatiitic melt. The resulting suites of plutonic-subvolcanic associations in the Serpentinite Belt–Tulppio Belt (or the SB–TB megastructure) defines a large igneous province [5,12].

Of the intrusive bodies along the SB–TB megastructure, only the Pados-Tundra complex has been dated: 2485 ± 38 Ma. As in the case of Lyavaraka and Pados-Tundra (Figure 1a), these dominantly ultrabasic bodies are not associated with coeval volcanic suites. They are thus distinct from others emplaced in the eastern Fennoscandian Shield that are roughly coeval and that have gabbroic members such as the Monchepluton complex [14] and volcanic equivalents. All of them, however, are anorogenic, formed in a stable within-plate environment in the interval 2.5–2.4 Ga [15,16]. They all are members of a large igneous province formed in the Sumian cycle of igneous activity [17].

Our earlier work on the Lyavaraka intrusive complex (Figure 1a,b) dealt with the chromian spinel and its unusual association with ilmenite [18,19]. Here, our objectives are (1) to examine the geological setting of the complex and its relationship with other suites of the Serpentinite Belt, (2) to complement the earlier findings [20,21] about the structure of the complex, and (3) to present new information on the composition of the rock-forming minerals and on the bulk composition of representative specimens. Our inferences lead to an improved understanding of the pattern of crystallization of the komatiitic melt at Lyavaraka, with possible implications for the other ultrabasic complexes of the Serpentinite Belt.
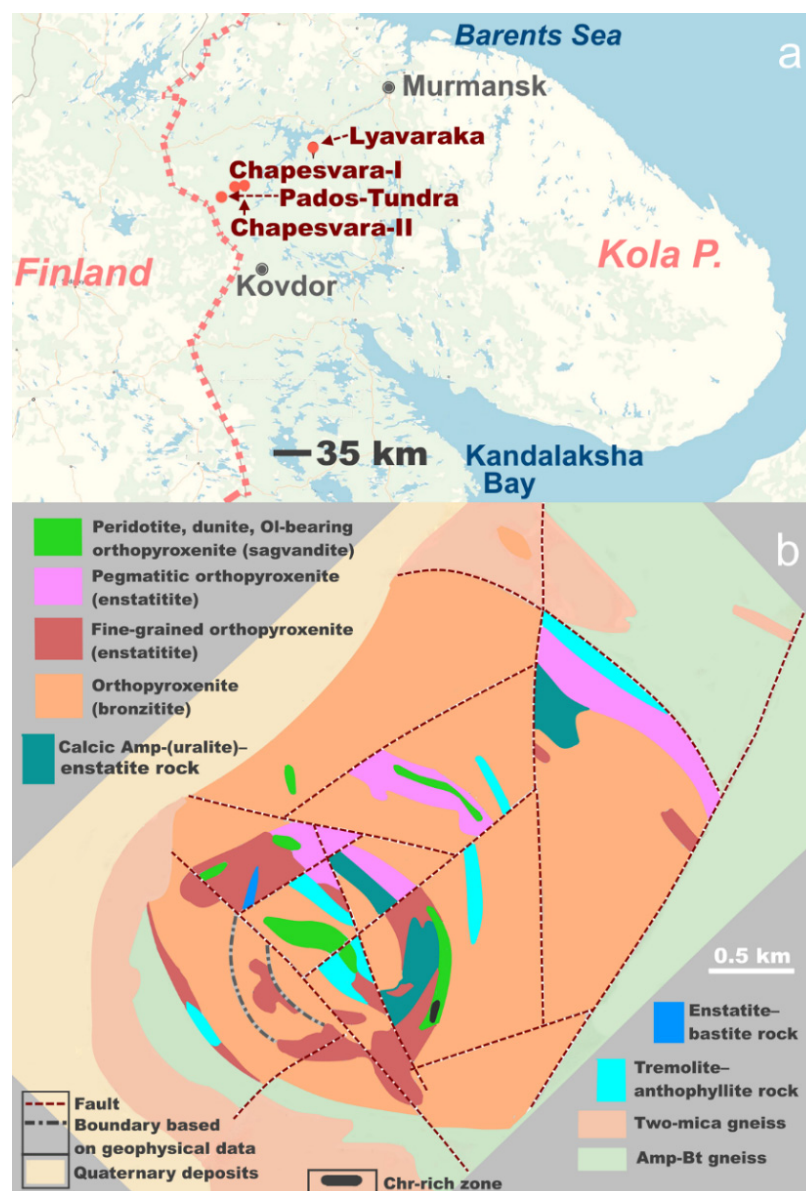


**Figure 1.** (**a**) shows the location of the Lyavaraka complex (68°25′ N, 31°32′ E) relative to the Pados-Tundra layered intrusion and Chapesvara (I and II) zoned sills, in the Kola Peninsula of northwestern Russia. (**b**) is a simplified geological map of the Lyavaraka complex, after [20]. All symbols used in Figure 1 and in the text conform to [22].

## 2. Materials and Methods

Our investigation of Lyavaraka is based on about fifty representative rock samples, from which one hundred polished sections were examined. The exposures sampled cover the entire complex (Figure 2). More than two thousand point-analyses were made at the

Analytical Center for Multi-elemental and Isotope Studies, SB RAS, Novosibirsk, Russia. Results of the analyses are presented in figures and in Supplementary Tables S1–S12.
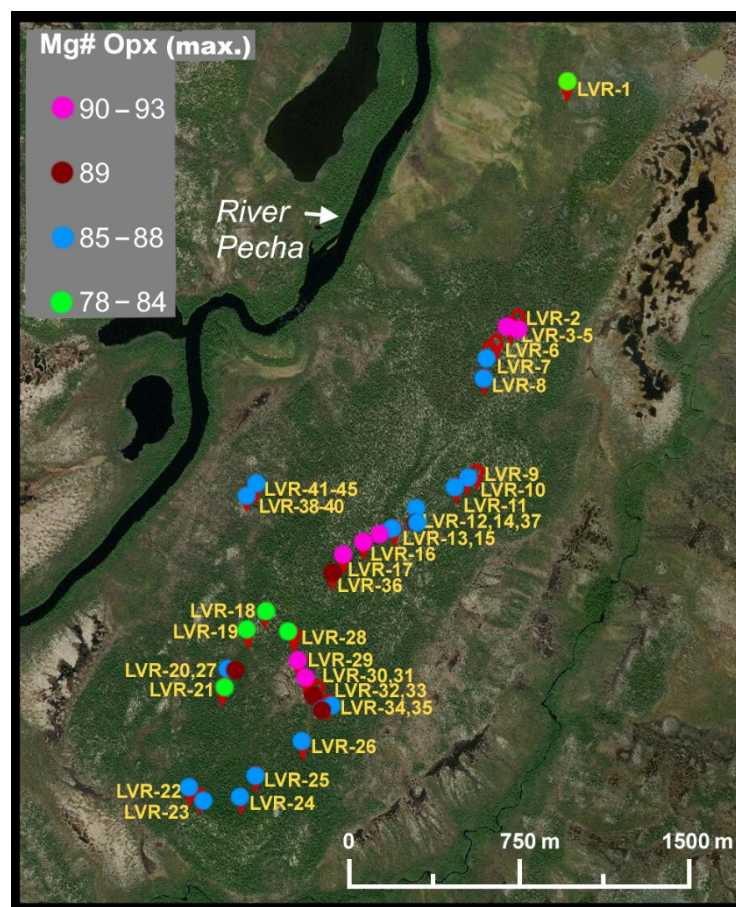


**Figure 2.** The location of our samples [18], plotted on a satellite image, is coded to indicate schematically the maximum value of the Mg# index, i.e., 100 Mg/(Mg + Fe + Mn), in orthopyroxene, Opx. The most primitive samples are cumulates, members of the ultrabasic core, here labeled Zone I: LVR29–35. The bulk of the samples pertain to the orthopyroxene-dominant Zone II (LVR1–17, 22–25, and 36–45). Sample LVR26, a pegmatitic orthopyroxenite, is located close to the inferred boundary with Zone I. Samples LVR18–20, 21, 27 and 28 are the most evolved, and they belong to Zone III, in which the olivine recurs, primocrysts of clinopyroxene appear, and late plagioclase is prominent.

The minerals were analyzed in the same center using a JEOL JXA-8100 instrument operated in the WDS mode. An accelerating voltage of 20 kV and a probe current of 30 to 50 nA were commonly used. We employed $K\alpha$ analytical lines for all elements except for Cr; the $K\beta_1$ line was used instead because of peak overlap. The measurements were made on the peaks for 20 or 10 s. The superposition of the Ti$K\beta_1$ line on the V$K\alpha$ line and of the V$K\beta$ line on the Cr$K\alpha$ line was accommodated using the overlap correction software. The beam diameter was ~1–2 μm. Natural specimens of olivine (Mg, Si, Fe, and Ni) and chromiferous or manganiferous garnet (Ca, Cr and Mn) were used as standards for olivine. Grains of orthopyroxene and hydrous silicates were analyzed using pyrope (Si, Al, Fe), a glass Ti standard (GL-6), chromiferous garnet (Cr), diopside and pyrope (Mg, Ca), manganiferous garnet (Mn), albite (Na), and orthoclase (K). All data were processed with the ZAF method of corrections. The calculated values of detection limit (1σ criterion) are: ≤0.01 wt.% for Ti, Cr, Fe, Ni, Ca, Zn, Mn, and K, and 0.02 wt.% (Na and Al). Other details concerning the accuracy and reproducibility of the analytical procedures were described by [23,24].

The sulfide minerals were analyzed at 20 kV and 50 nA using a finely focused beam (~1 μm), the standard Phi-Rho-Z procedure and the following lines (and standards): Fe$K\alpha$,

$CuK\alpha$, $SK\alpha$ ($CuFeS_2$), $CoK\alpha$ and $NiK\alpha$ (synthetic FeCoNi alloy); the minor overlap of the $FeK\beta$ line with the $CoK\alpha$ line was corrected. The scapolite grains were analyzed with a 2-μm beam at 20 kV and 30 nA, using standard specimens of fluorapatite ($FK\alpha$), chlorapatite ($ClK\alpha$), chalcopyrite ($SK\alpha$), albite ($NaK\alpha$), Fe-bearing pyrope ($MgK\alpha$, $FeK\alpha$), orthoclase ($KK\alpha$, $AlK\alpha$, $SiK\alpha$), manganiferous garnet ($MnK\alpha$), synthetic $BaSiO_3$ ($BaL\alpha$) and $SrSiO_3$ ($SrL\alpha$), diopside ($CaK\alpha$), and Ti-bearing chromite ($CrK\alpha$, $TiK\alpha$). The ZAF procedure was used; the Ti–Ba peak overlaps were corrected.

Whole-rock major- and trace-element analyses were also performed in the Analytical Center for Multi-elemental and Isotope Studies. Contents of major and minor elements were established via X-ray fluorescence analysis (XRF) using the instrument ARL-9900XP (Thermo Fisher Scientific Ltd., Waltham, MA, USA). Levels of high-field-strength elements (HFSE), including the rare-earth elements (REE), were measured by high-resolution inductively coupled plasma–mass spectrometry (ICP-MS) using the instrument ELEMENT (Finnigan MAT, San Jose, CA, USA). Analytical details have been described [25–27].

## 3. Results

### 3.1. Geological Setting

Figure 3 shows the general context of the study area and its relation to the main tectonic elements of the Kola Peninsula. Figure 4 provides a summary of regional-scale maps; the Lyavaraka intrusion and the Serpentinite Belt are adjacent to the younger Tanaelv high-grade ductile thrust belt and collision mélange. The Tanaelv structure underlies rocks of the Lapland granulite terrane forming part of the Paleoproterozoic Lapland–Kola orogen [28,29].
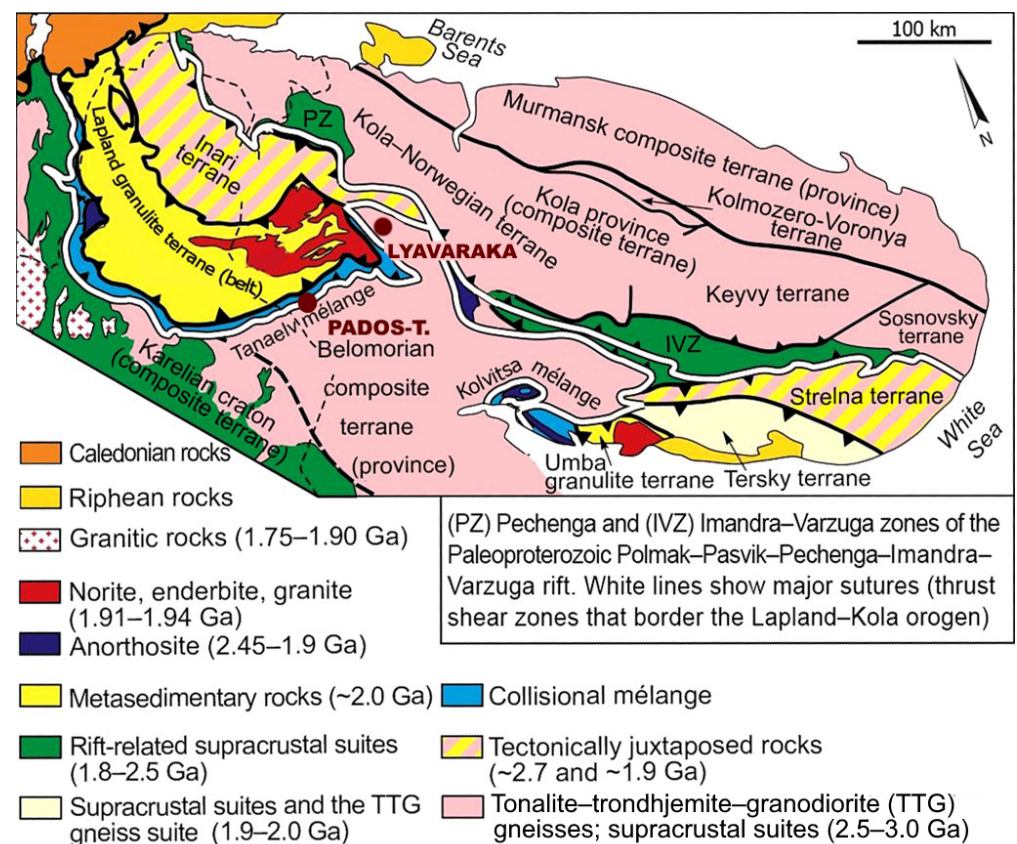


**Figure 3.** Location of the Lyavaraka and Pados-Tundra complexes, shown in the context of tectonic elements of the northeastern part of the Fennoscandian Shield, after [28] and references therein.
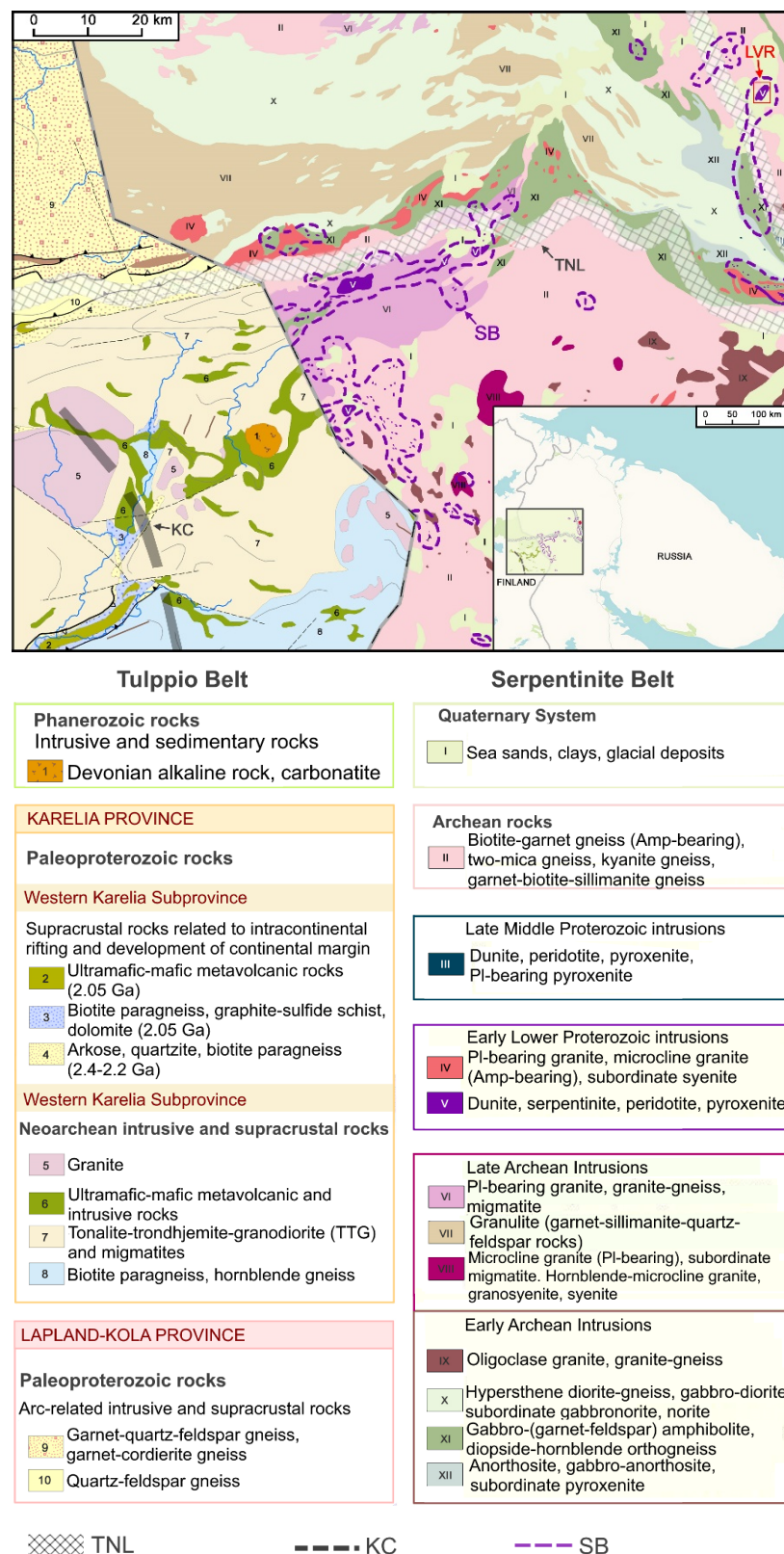
**Figure 4.** The location and geological setting of the Lyavaraka complex (LVR) relative to other suites of ultrabasic rocks of subvolcanic plutonic complexes of the Serpentinite Belt (SB), all containing the association dunite–harzburgite–orthopyroxenite. The map shows the geological context in the Fennoscandian Shield, compiled on the basis of various sources in the literature: references [30–34] for the Russian part and references [35,36] for the complementary Tulppio Belt in Finland. Boundaries of the Tanaelv high-grade ductile thrust belt (TNL) and of the Karelian Craton (KC) are shown schematically.

The Lyavaraka body is one of the dunite–harzburgite–orthopyroxenite associations of the Serpentinite Belt (Figure 4). Note that a different stratigraphic position is presently accepted for related suites of the Tulppio Belt in Finland, which are assigned a Neoarchean age [35,36]. The ultrabasic suites of the Serpentinite Belt appear to be Paleoproterozoic on the basis of geological relations [30–34] and results of Sm–Nd dating of the Pados-Tundra layered complex: $2485 \pm 38$ Ma [10].

### 3.1.1. Exposures and Significant Petrographic Details

Outcrops at Mount Lyavaraka typically are steep, rounded blocks from ~2–3 up to tens of meters across; groups of blocks are common in the central portion of the complex (Figure 5a,b). In addition, there are terrace-like relatively denuded areas, with large exposures of orthopyroxenite related to a stepped descent toward the River Pecha basin.



**Figure 5.** (**a**,**b**) Typical exposures of ultramafic rocks in the Lyavaraka complex. In the background of (**b**), S.S. Kramzaev stands near a large and sloping outcrop of pegmatitic Opx–Amp rocks.

Dunitic to harzburgitic rocks make up only a minor proportion of the exposures at Lyavaraka. Orthopyroxenite is volumetrically dominant (Figure 2); it ranges from fine-grained to pegmatitic (Figure 6a,b). It occurs not only at the northern contact, as mapped previously (Figure 1b), but also at the southern contact, especially in the area close to our sample LVR-23 (Figure 2).



**Figure 6.** (**a**,**b**) Characteristic examples of megaspheroidal orthopyroxene (Opx), resorbed and converted to amphibole to various extents, as observed in pegmatitic facies at the southern contact of the Lyavaraka intrusion. The label Amp refers to amphibole.

Orthopyroxene is a subordinate constituent of the dunitic to harzburgitic rocks (Figure 7a), which make up the Ultrabasic Core-like Zone (UBC Zone I), briefly described below. Orthopyroxene is the major mineral in the other more evolved units, labeled Zone of Opx II and Zone of Recurrent Ol + Cpx + Pl (ROCP III).
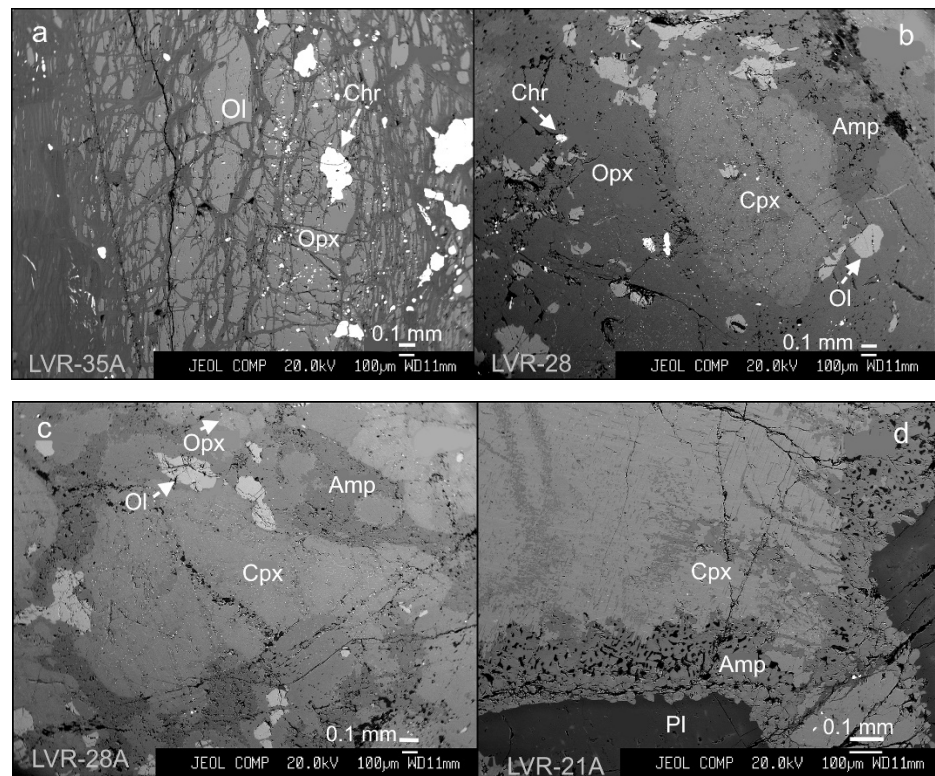
**Figure 7.** (**a**–**d**) Back-scattered electron (BSE) image of a sample of texturally massive dunite from Zone I, only slightly serpentinized, grading to harzburgite (**a**). It consists mainly of magnesian olivine (Ol) with subordinate grains of Opx and abundant grains of chromian spinel (Chr). (**b**,**c**) display occurrences in Zone III of small grains of recurrent olivine (Ol) adjacent to large grains of magnesian clinopyroxene (Cpx) associated with orthopyroxene (Opx). The term *recurrent* expresses clearly the fact that olivine appears anew after an interval in which it had ceased crystallizing. A reaction rim of amphibole (Amp) of pargasitic composition, also in Zone III, contains submicrometric symplectitic inclusions of quartz (black in (**d**)). Such rims develop in clinopyroxene (Cpx) along its contact with intercumulus plagioclase (Pl).

The existence of two generations of olivine is evident from our findings. The first generation is represented by grains of fairly high-Fo olivine (Figure 7a) in dunite, harzburgite and Ol-bearing orthopyroxenite of Zone I. The second generation of lower-Fo olivine occurs as irregular grains that appeared after the primocrystic grains of highly magnesian clinopyroxene (Figure 7b,c). These grains of clinopyroxene, intercumulus plagioclase and Cl-bearing scapolite (Figure 8d) are found in Zone III, described below.
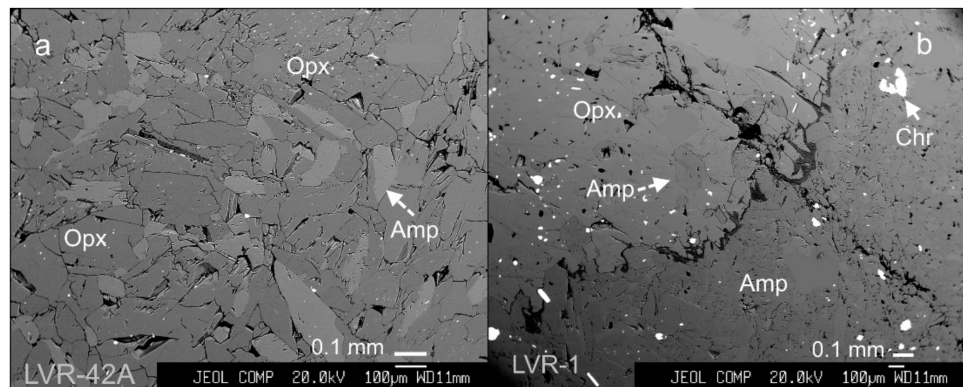


**Figure 8.** *Cont.*
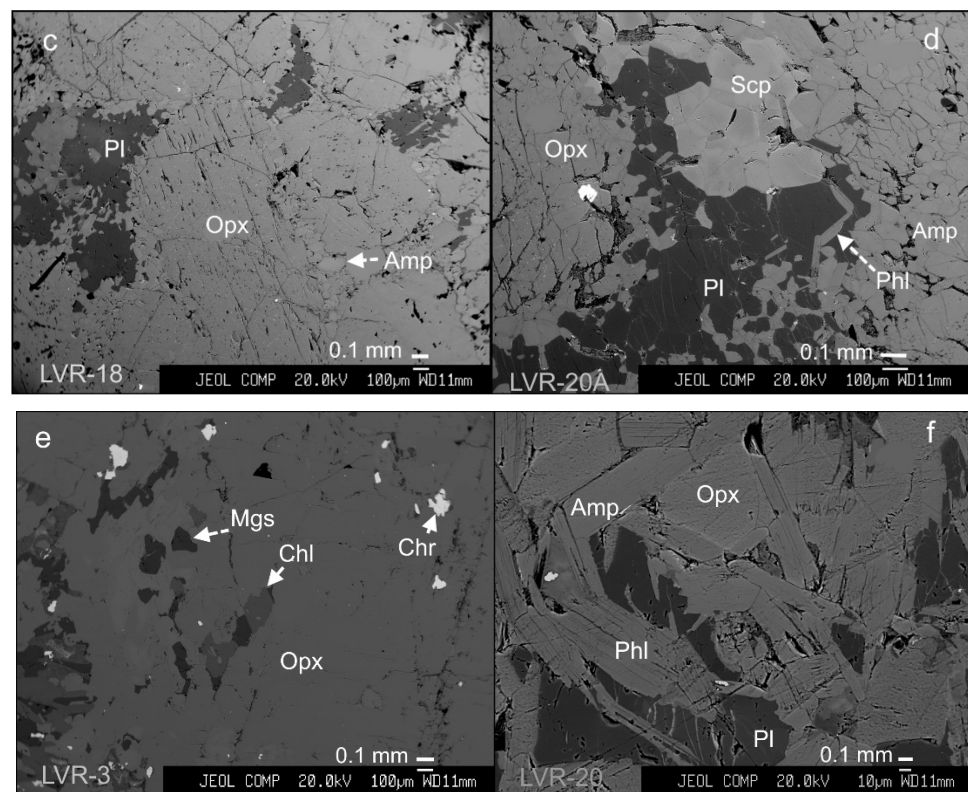
**Figure 8.** (**a**–**f**). A BSE image in (**a**) shows a sample of fine-grained orthopyroxene (Opx) coexisting with calcic amphibole (Amp). (**b**) displays a large grain of fairly fresh Opx, with inclusions of Amp, which is in contact with a compact aggregate of Amp grains; the label Chr points to accessory grains of chromian spinel. Grains of Opx (**c**) host irregular patches of plagioclase (Pl) and are replaced by Amp along the rim. Subhedral grains of interstitial plagioclase (Pl) fill the space between a large grain of Opx and an amphibole-based aggregate (Amp). Note the presence of abundant grains of scapolite (Scp) (**d**) associated with the plagioclase and platy grains of phlogopite (Phl). (**e**,**f**) show late assemblages of deuterically deposited magnesite (Mgs), a member of the chlorite group, Chl (corresponding to clinochlore), phlogopite (Phl), and amphibole (Amp), which are associated with orthopyroxene (Opx).

Three types of amphibole are observed. The first type is calcic amphibole, mainly tremolite varying to actinolite and magnesio-hornblende that is more or less subordinate. In many cases, tremolite seems to be a primary phase, coexisting with fine-grained orthopyroxene (Figure 8a). The second type is a Mg–Fe amphibole corresponding to anthophyllite. The latter Amp is associated with the calcic amphiboles, which can both form zoned grains. These amphiboles largely postdated the formation of orthopyroxene, and replaced it during a stage of autometamorphic activity. Similar relationships were previously noted for the Opx–Amp associations in other complexes in the Serpentinite Belt [5,6,8,12,13]. The third type of amphibole, pargasite, formed as a result of local reactions involving a hydrous fluid with primary grains of Cpx and Pl. The $SiO_2$ produced in these reactions appears in a symplectitic intergrowth (Figure 7d).

### 3.1.2. Compositional Variations in the Lyavaraka Complex

Representative results of wavelength-dispersive electron-microprobe analyses of the main minerals are plotted in Figures 9–12 and provided in supplementary documents (Tables S1–S12). Olivine of the first generation (Zone I) has Mg# in the range 89.1–90.3 in the core-like zone (Figure 9). Such a composition corresponds to the typical level of magnesium enrichment in olivine recorded in early differentiates of large bodies of the Serpentinite Belt. For example, in Zone I of the Khanlauta flow, which is less than 0.2 km

thick, olivine is slightly less strongly magnesian (Mg# 87.9). The maximum values of Mg# are encountered in zones of chromite mineralization of the Dunite block at Pados-Tundra ($Fo_{93}$) and in the Upper Contact Facies of the Chapesvara sill ($Fo_{92}$) [5,9,12]. In contrast, olivine of the second generation (Zone III) is significantly enriched in iron (Mg# 74.5–75.8), with greater levels of Mn (Figure 9, Table S1).
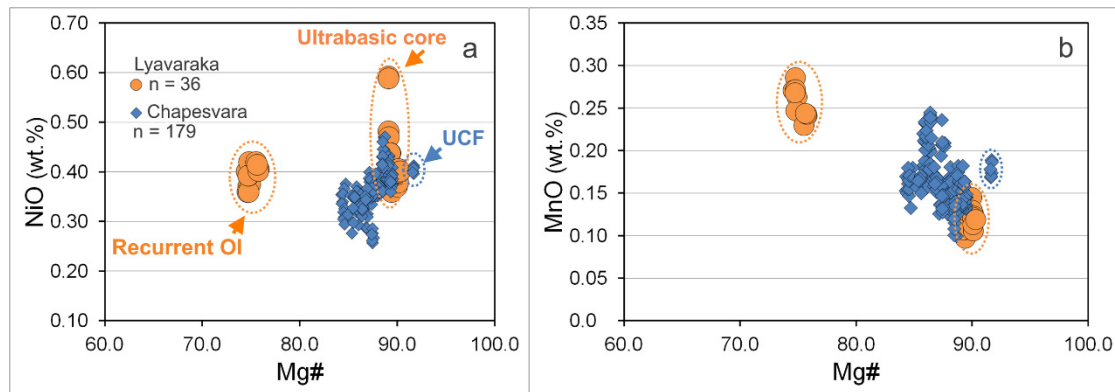


**Figure 9.** (**a**,**b**). Plot of values of the Mg# index, i.e., 100 Mg/ (Mg + $Fe^{2+}$ + Mn) in olivine versus contents of NiO (**a**) and MnO (**b**), both expressed in weight %, in WDS compositions of grains from the Lyavaraka complex (orange symbol; this study) compared with olivine from the Chapesvara complex, Serpentinite Belt (blue symbol), after [12]. The number of WDS data-points (n) is reported in (**a**). The label UCF refers to the Upper Contact Facies [12].

Orthopyroxene grains vary in composition from Mg# 75.7–78.2 to a maximum of 93.0 (Table S2), which slightly exceeds the degree of magnesium enrichment of Opx in all of other complexes of the belt, including the Pados-Tundra complex: $En_{91}$ [6]. Levels of Cr incorporated in the orthopyroxene commonly attain 1 wt.% $Cr_2O_3$, but rarely attain the maximum (1.5–1.6 wt.% $Cr_2O_3$) in the Dunite block and other geological units of the Monchepluton complex in the Kola Peninsula [9]. The observed range of Opx compositions is much greater than that established in the Chapesvara complex (Figure 10). On the other hand, compositions of clinopyroxene at Lyavaraka, i.e., diopside $Wo_{45.2–48.0}En_{42.9–45.2}Fs_{5.9–8.3}Aeg_{1.9–3.1}$ with Mg# 81.1–88.0 (Table S3), are similar to those in the Chapesvara sill (Figure 11).
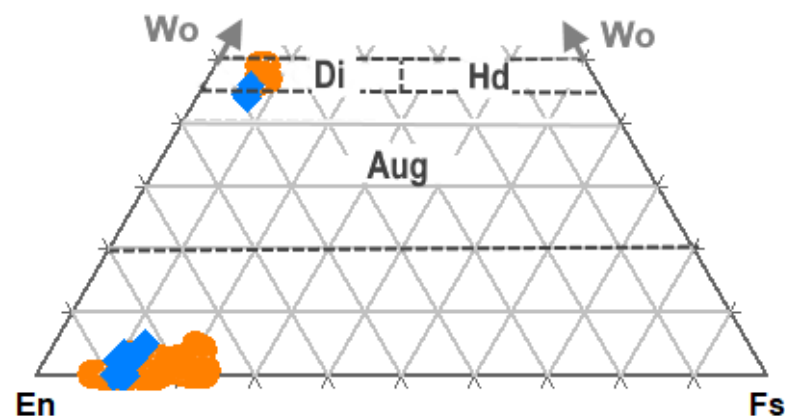


**Figure 10.** The Ca–Mg–Fe plot displays a comparison of compositional variations in orthorhombic and monoclinic pyroxenes from the Lyavaraka complex (this study) vs. those reported from the Chapesvara sill [12], shown by the orange and blue symbols, respectively. The symbols used are: Wo, wollastonite; En, enstatite; Fs, ferrosilite; Aug, augite; Di, diopside; and Hd, hedenbergite. The nomenclature and mineral names are after [37].
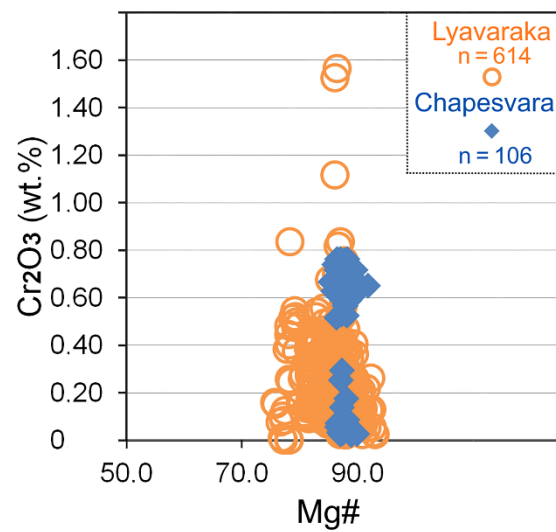
**Figure 11.** Plot of values of the Mg# index, i.e., 100 Mg/ (Mg + Fe$^{2+}$ + Mn), vs. contents of Cr$_2$O$_3$ in WDS compositions of orthopyroxene from the Lyavaraka complex (orange symbol) compared with those from the Chapesvara complex, Serpentinite Belt (blue symbol), after [12].

Compositions of intercumulus grains of plagioclase in Zone III vary from An$_{48.5}$ to An$_{13.1}$ (Ab$_{86.7}$) in the Lyavaraka complex (Table S4). The calcic members of the series are close to An$_{39.7–53.0}$ in the Chapesvara complex, in which Cpx and Pl also are involved in a reaction relation: Cpx → Pl → aluminous Amp (pargasite) [12].

The overall variation in the composition of the amphiboles is displayed in Figure 12, in which these are compared with the related series documented in the Chapesvara sills [12]. All are plotted on the same linear trend in terms of contents of Si and Al (Figure 12a). Two major groups of amphibole are recognized (Figure 12b): calcic amphiboles, mostly tremolite and subordinate magnesio-hornblende (Table S5), and the Mg–Fe amphibole, corresponding to anthophyllite (Table S6). Compositions of pargasite vary little (Table S7).
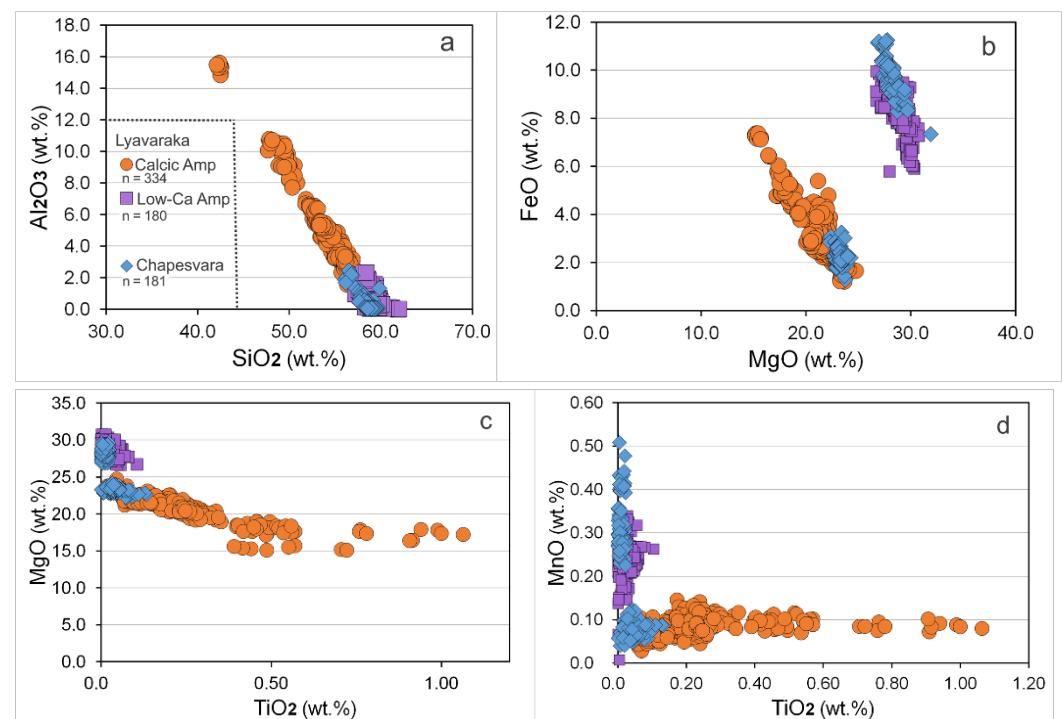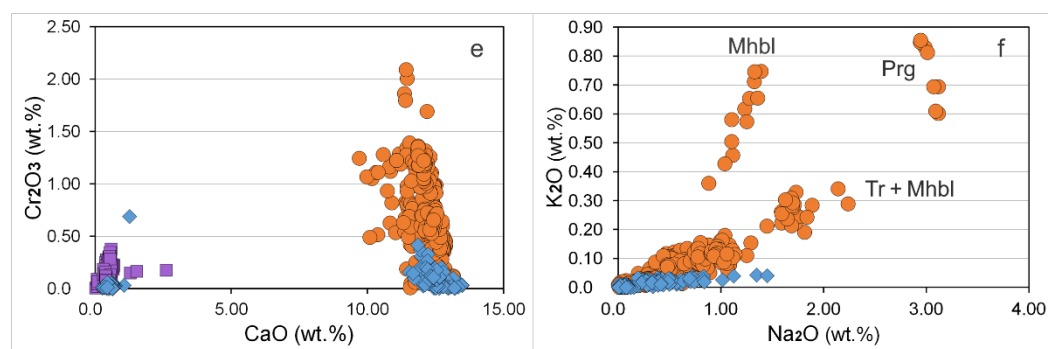


**Figure 12.** *Cont.*

**Figure 12.** (**a**–**f**). Plot of contents of SiO$_2$ vs. Al$_2$O$_3$ (**a**), MgO vs. FeO (**b**), TiO$_2$ vs. MgO (**c**), TiO$_2$ vs. MnO (**d**), CaO vs. Cr$_2$O$_3$ (**e**), and Na$_2$O vs. K$_2$O (**f**), all expressed in weight %, in WDS compositions of amphiboles from the Lyavaraka complex (this study, orange circles), compared with those of amphiboles from the Chapesvara complex (blue diamond symbol; after [12]). WDS compositions of low-calcium Mg–Fe amphiboles of the Lyavaraka complex are shown by purple squares. The symbols Tr, Mhbl and Prg stand for tremolite, magnesio-hornblende and pargasite, respectively.

Two additional trends are worthy of note. One involves an enrichment in Ti in the calcic amphibole, and the second pertains to a relative enrichment in Mn in the Mg–Fe amphibole (Figure 12c,d). Note that the calcic amphibole is the preferred host of Cr among silicates at Lyavaraka (Figure 12e); the Cr-enrichment of the Amp grains exceeds the corresponding levels in the associated orthopyroxene. Notable similarities are observed in the compositional trends of the associations at Lyavaraka and Chapesvara. The amphibole at Lyavaraka displays more pronounced variations, with greater enrichment in Fe, Ti, Cr and Na (Figure 12c,e,f). Elevated levels of K are uncommon and present only in some members of the compositional series of magnesio-hornblende and pargasite (Figure 12f).

Interestingly, scapolite occurs in a close association with plagioclase and phlogopite in Zone III (Figure 8d). Its content of Cl, analyzed in different portions of grains, varies slightly around 1 wt.% (Table S8). Compositions of phlogopite are enriched in Ti (up to 4 wt.% TiO$_2$), Cr (1.4 wt.% Cr$_2$O$_3$) and Na (1.3 wt.% Na$_2$O) (Table S9).

In general, rocks of the complex are extremely poor in sulfide minerals. Tiny grains ($\leq 20$ μm) of accessory base-metal sulfides were found and analyzed in orthopyroxenite samples in the southwestern part (Table S10). The relative abundance of Co-bearing pentlandite, the main species of sulfide, agrees well with observations from other representatives of the Serpentinite Belt [5,12,13]. Two phases of uncommon compositions, i.e., $(Cu,Fe)S_{2-x}$ and $(Fe_{0.55}Cu_{0.5})S_2$ (#1–3 in Table S10), may represent a variant of villamanínite enriched in Fe and a pyrite-type member of the FeS$_2$–CuS$_2$ solid solution, i.e., an analog of synthetic $(Fe_{0.6}Cu_{0.4})S_2$ [38], respectively. In addition, grains of chalcopyrite and troilite occur sporadically.

Parageneses of chromian spinel and ilmenite at Lyavaraka were documented previously [18,19].

### 3.1.3. Geochemical Variations in the Lyavaraka Complex

The rocks of Zone I of the Lyavaraka complex are compositionally relatively primitive and magnesian (Table S11). The mean values of Mg#, calculated on a whole-rock (molar) basis, are nearly identical at Lyavaraka (86.4; *n* = 33), Chapesvara-I (86.6) and Chapesvara-II (86.5) sills, and the Khanlauta flow (86.1), values that are all very close to that reported for the Pados-Tundra complex (87.6) [5,12,13].

Rocks of Zone III (e.g., samples LVR 18–21, 28), as discussed below, display the following bulk-rock variations: CaO 3.18–8.70 wt.%, Al$_2$O$_3$ 4.37–7.65%, Na$_2$O 0.62–1.14%, and K$_2$O 0.20–0.40%, with Mg# 77.5–85.2 and MgO/SiO$_2$ (molar ratio) 0.58–0.75. These values point to a more evolved (fractionated) state of rocks in Zone III relative to the two other units of the complex. This inference is corroborated by extents of relative enrichments

in levels of incompatible elements, including the REE and HFSE (Table S12), along with the mineralogical data presented.

The geochemical variations, trends and relationships documented for Lyavaraka are compared with those from the Chapesvara and Khanlauta suites (Figures 13–16). These complexes all appear to be comagmatic. The CI–chondrite-normalized plots (Figure 17a,b) are also very similar [5,12,13]. The Mg vs. Ni correlation is sympathetic (Figure 13a), as expected in view of the high dominance of silicates over Ni-based sulfides. The minor deviation from the trend is attributed to the presence of minor amounts of Ni sulfide. The predominance of orthopyroxene over olivine at Lyavaraka accounts for the comparatively low levels of Ni (Figure 13a).
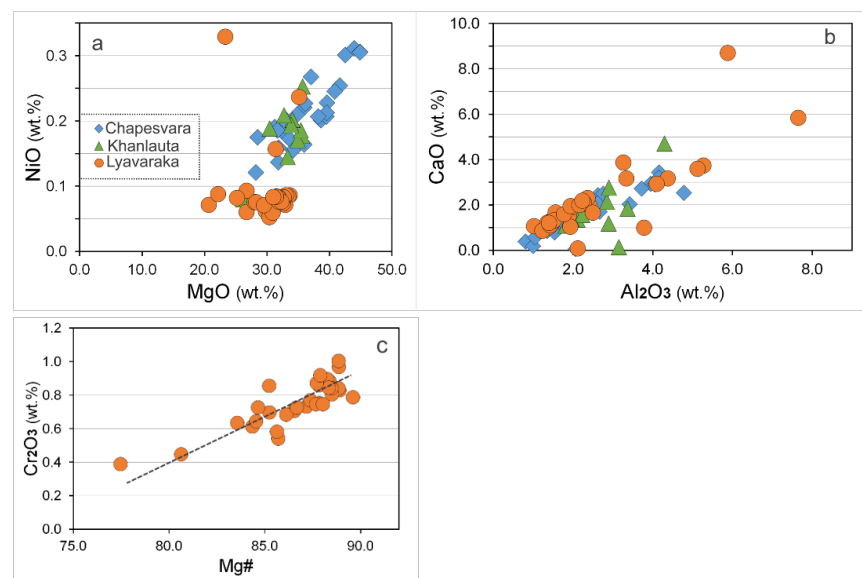


**Figure 13.** (**a**–**c**). Plot of contents of MgO vs. NiO in wt.% (**a**), $Al_2O_3$ vs. CaO in wt.% (**b**), and values of the Mg# vs. contents of $Cr_2O_3$ in wt.% (**c**), in ultrabasic rocks of the Lyavaraka complex (orange symbols), compared with the Chapesvara sill [12] (blue diamonds) and the Khanlauta differentiated flow [13] (green triangles).
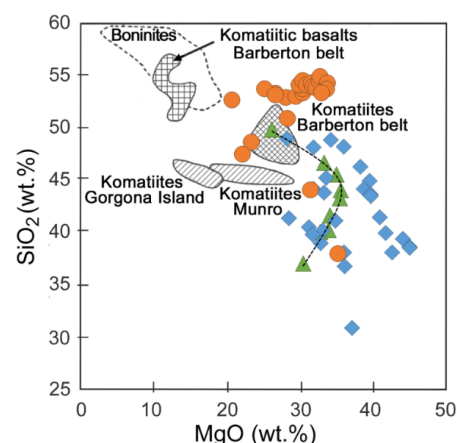


**Figure 14.** Plot of bulk-rock contents of MgO vs. $SiO_2$ (wt.%) showing compositional variations of the Lyavaraka complex (orange symbol; this study) compared with the compositional field of the Chapesvara complex [12] (blue symbol) and with the linear trend reported for the differentiated flow of the Mount Khanlauta complex [13] (green symbol). Additionally, shown for comparison are schematic boundaries of typical fields of boninites, komatiitic basalts and komatiites of the Barberton Belt in South Africa, Gorgona Island in Columbia, and the Munro area in Ontario, Canada, after [39].
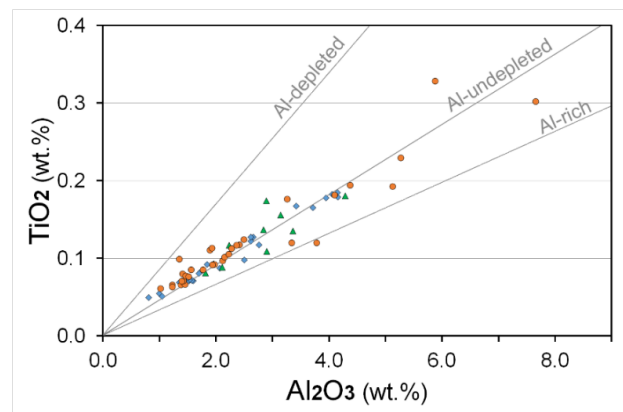
**Figure 15.** Plot of bulk-rock contents of $Al_2O_3$ vs. $TiO_2$ both expressed in weight %, showing compositional variations of the Lyavaraka complex (orange symbol; this study) compared with the compositional field of the Chapesvara complex [12] (blue symbol) and the differentiated flow of the Mount Khanlauta complex [13] (green symbol). Schematic trends of the Al-depleted, Al-undepleted and Al-rich komatiites are shown for comparison, after [40].
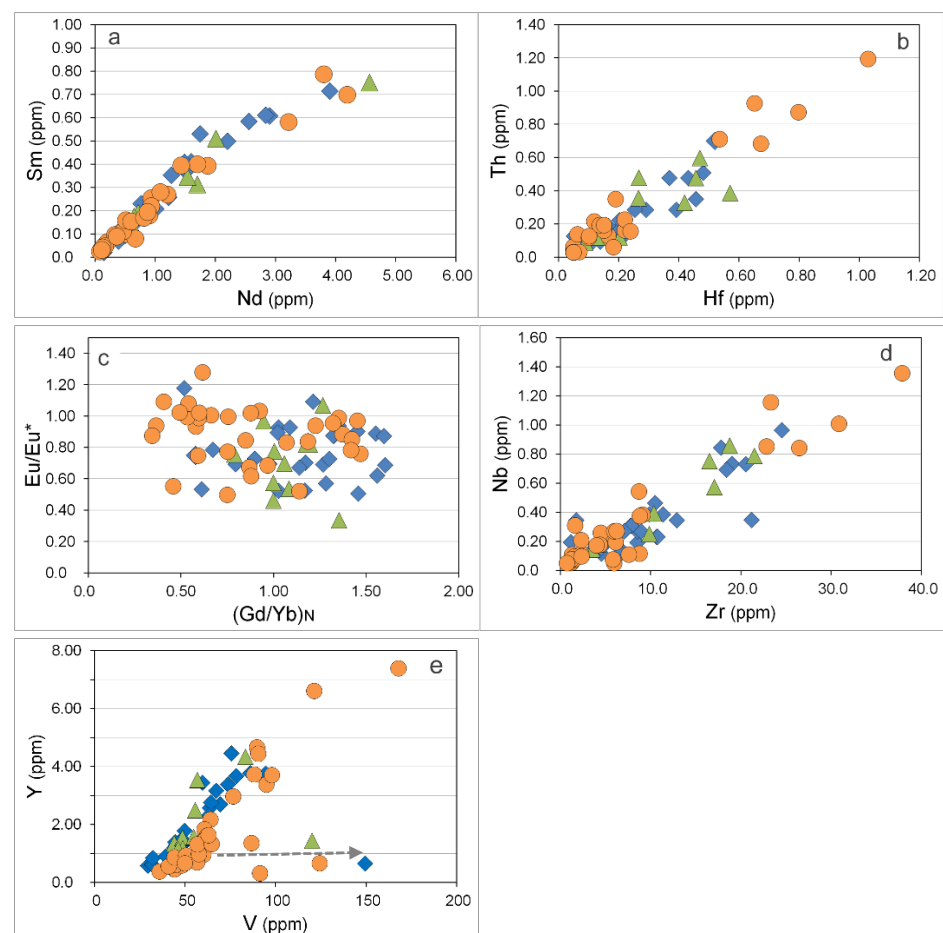


**Figure 16.** (**a**–**e**). Plot of values of Nd vs. Sm (**a**), Hf vs. Th (**b**), values of the indexes $(Gd/Yb)_N$ vs. Eu/Eu* (**c**), Zr vs. Nb (**d**) and V vs. Y (**e**) expressed in ppm in whole-rock compositions of ultrabasic rocks of the Lyavaraka complex (orange symbol), compared with the related suites of the Chapesvara sill [12] (blue diamonds) and the Khanlauta differentiated flow [13] (green triangles). The dotted arrow in Figure 16e shows the trend of relative V-enrichment caused by the presence of accessory oxide minerals (chromite and ilmenite).
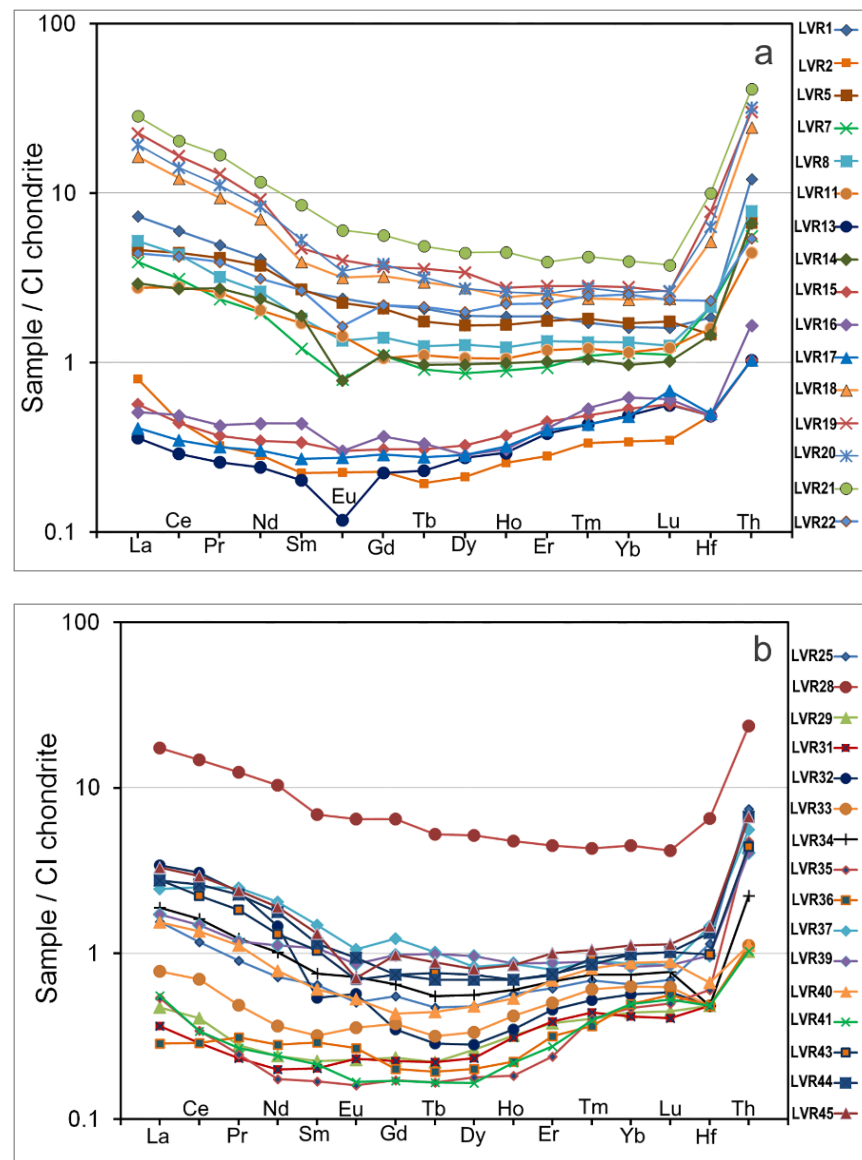
**Figure 17. (a,b).** The CI–chondrite-normalized contents of lanthanides, Hf and Th [41] in the ultrabasic rocks of the Lyavaraka complex. As indicated in the caption to Figure 2, samples LVR29–35 constitute Zone I, LVR1–17, 22–25 and 36–45 are in Zone II, with LVR26 located close to the boundary with Zone I, and samples LVR18–20, 21, 27 and 28 belong to Zone III.

The sympathetic relationships of Ca and Al (Figure 13b) reflect their mutual accumulation in the melt as crystallization progressed. The comparatively greater degrees of fractional crystallization at Lyavaraka led to the observed crystallization of clinopyroxene and, at a late stage, plagioclase in Zone III.

No clear relationship is observed between the level of magnesium enrichment and Cr content of Opx grains at Lyavaraka (Figure 11). Nevertheless, except for the Chr-mineralized samples, chromium behaves rather compatibly, as is shown by the positive correlation evident in Figure 13c, in which the whole-rock Mg# index is plotted as a function of level of $Cr_2O_3$, expressed in wt.%.

In terms of a plot of MgO vs. $SiO_2$ (Figure 14), the Lyavaraka whole-rock compositions generally cluster into a separate field that is fairly close to that characteristic of komatiites of the Barberton Belt in South Africa [39]. Note that the Lyavaraka sequences exhibit, in the $Al_2O_3$ vs. $TiO_2$ diagram (Figure 15), the same trend as the Chapesvara and Khanlauta suites, consistent with an Al-undepleted komatiitic magma. Additionally, note that rocks

of Zone III are notably enriched in Al ($Al_2O_3$ 4.37–7.65 wt.%), and these account for the high values observed in Figure 15.

Variation diagrams in Figure 16a–e show systematic trends and patterns of selected pairs of minor and trace elements, including REE and HFSE. These provide further comparisons of the Lyavaraka successions with those in related suites of komatiitic origin at Chapesvara and Khanlauta. These trends are all notably similar. In addition, rocks of Zone III attain the maximum concentrations of the incompatible elements, such as expressed in the plots of Th vs. Hf (Figure 16a), Zr vs. Nb (Figure 16d), and V vs. Y (Figure 16e). The chondrite-normalized spectra of the Lyavaraka successions (Figure 17a,b) are similar to the patterns reported from Chapesvara, Khanlauta, and to those of the Pados-Tundra layered complex [5,12,13]. The greatest abundances of all rare-earth elements are found in samples of Zone III: LVR 18–21, 28 (Figure 16a,b).

## 4. Discussion

### 4.1. Geotectonic Inferences and Implications for Primary Melts

A review of the geological data (Figures 3 and 4) indicates that the Lyavaraka intrusion is one of numerous bodies that belong to the Serpentinite Belt (SB). The overall length of the SB exceeds 200 km in Russia [42]. The addition of suites of the complementary Tulppio Belt (TB) as an important component of the SB–TB structure (Figure 4) extends it considerably. As noted, a Paleoproterozoic age is assigned to Lyavaraka by analogy with the Pados-Tundra complex [10]; thus, along with other SB–TB representatives, they seem to be synchronous (2.5–2.4 Ga) with komatiitic suites of the Vetreny Belt [17,43] and layered intrusions of the Fennoscandian Shield [44,45].

We contend that Lyavaraka and the other members of the Serpentinite Belt formed from a komatiitic magma. The Mg# value of olivine attains 89.1–90.3 with up to 0.6 wt.% NiO at Lyavaraka, and 92 in the uncontaminated fine-grained contact facies at Chapesvara-II [12]. The magma forming the chilled margin is inferred to contain approximately 22 wt.% MgO. The label *komatiitic* is applied if the magma contains at least 18% MgO [46].

These subvolcanic-plutonic komatiitic suites [5,12,13] result from the emplacement of large volumes of Al-undepleted komatiitic magma derived from a large-scale mantle plume. The magma reached shallow zones in the crust to form the ultramafic sills and shallow plutonic rocks of highly magnesian composition. The associated sills of the Chapesvara and Lotmvara complexes are controlled by systems of shear zones with a north-northeasterly strike [5,12,13]. The same geological setting seems likely for the Lyavaraka intrusion, which also exhibits a northeasterly strike (Figure 1b, Figure 2, and Figure 4).

The Pados-Tundra and Chapesvara complexes, which show the maximum degree of magnesium enrichment in olivine ($Fo_{93}$ and $Fo_{92}$, respectively), could represent the central portion of an inferred mantle plume [5]. The Lyavaraka intrusion is located most remotely from this "center" (Figure 4). This is consistent with the more extensive fractional crystallization achieved at Lyavaraka, resulting in the mineralogical and geochemical characteristics of Zone III. Interestingly, some of the other ultrabasic complexes, such as Yanesvaara, Tepsi-Tundra and Urochishche Tepsi, along the southern branch of the SB, also are located remotely with respect to the inferred plume head.

The following mineralogical evidence suggests that the parental Al-undepleted komatiitic magma had an elevated content of volatiles, $H_2O$ and $CO_2$. (1) Orthopyroxene typically coexists with grains of high-Mg amphibole (typically tremolite). The cocrystallization of these minerals in fine-grained orthopyroxenite (Figure 8a) is consistent with an $H_2O$-saturated melt in Zone II. (2) The presence and abundance of a pegmatitic facies at Lyavaraka results from the extensive degassing of the primary melt, leading to the accumulation and migration of a volatile-rich fluid phase toward an internal contact. The development of huge spheroidal grains of orthopyroxene, up to 12–15 cm in diameter (Figure 8a), is especially significant. These recall the spheroidal grains of talc and tremolite documented in the Pados-Tundra complex, which formed by the deuteric replacement of precursor Opx grains, or of oikocrysts of Opx in the Monchepluton complex in the

matrix of fresh grains of Ol [8]. (3) The assemblages of autometamorphic secondary minerals such as clinochlore, phlogopite, talc, magnesite, serpentine, Mg-rich members of the tremolite–actinolite series, magnesio-hornblende, anthophyllite, pargasite and scapolite are prominent. The scapolite invariably contains about 1 wt.% Cl (Table S8), and thus represents one more Cl-bearing mineral associated with several basic–ultrabasic complexes [47]. In addition, note that rocks of the Upper Contact Facies (UCF) of the Chapesvara sill consist of spherules of talc and Cr-enriched clinochlore up to 5 mm in diameter. The elevated level of $H_2O$ in the highly magnesian magma is also indicated by two uncommon features reported from the Serpentinite Belt: the development of a laurite–clinochlore intergrowth in mineralized dunite of the Pados-Tundra complex [7] and of oriented lamellae of primary clinochlore in grains of chromian spinel in the Chapesvara complex [15]. These observations suggest the likely existence of "hydrous high-MgO melts" [48,49].

A progressive buildup in levels of $fO_2$ is evident from detailed studies of the oxide parageneses at Lyavaraka [18,19]. In addition, the abundance of hematite, observed in the Khanlauta flow, is consistent [13]. We attribute it to the saturation of the magma in $H_2O$, which dissociates to release $H_2 + O_2$ during degassing in a shallow setting [50].

The point of inflection corresponding to the middle of the linear trendline that displays the path of crystallization of the Khanlauta flow (Figure 14) also corresponds to the hypothetical center for the entire field of compositions at Lyavaraka and Chapesvara. It seems likely that this point, with ~36 wt.% MgO and ~44 wt.% $SiO_2$, approximates the composition of the parental melt of the Serpentinite Belt. Indeed, the observed composition of the UCF at Chapesvara gave 37.04 wt.% MgO [12], which fits this suggestion well, but differs in too low a value of $SiO_2$, 30.95 wt.%, and a high Cr content. Saturation of the melt in the volatiles inferred above explains how the komatiitic melts of the Serpentinite Belt, which seem to be among most magnesian variants in a worldwide context [17,39,40,43,51–54], decrease their liquidus sufficiently to reach near-surface levels of emplacement. We reiterate that they crystallized in a stable cratonic environment in a within-plate setting.

### 4.2. Internal Structure, Zones and Crystallization of the Lyavaraka Complex

On the basis of our findings and the preliminary geological map [20], we recognize the existence of three structural units in the Lyavaraka complex. The three zones, shown schematically (Figure 18), are Zone I, an ultrabasic core-like zone, Zone II of dominant orthopyroxenite, and Zone III, in which the olivine recurs, primocrysts of clinopyroxene appear, and late plagioclase is prominent. The characteristics of each zone are briefly described in Table 1.
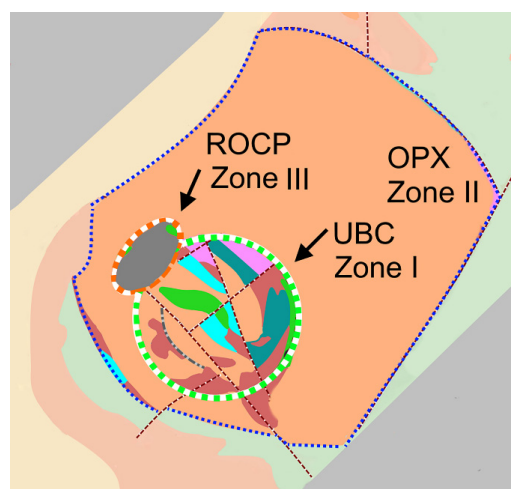


**Figure 18.** A generalized scheme of the geological structure of the Lyavaraka complex is based on our findings and results of previous mapping [16]. Three zones, shown schematically, are suggested: the Ultrabasic Core-like Zone (I), the Zone of Opx (II) and the Zone of Recurrent Ol + Cpx + Pl (III). See Table 1 for details.

**Table 1.** Major structural units of the Lyavaraka ultrabasic intrusion.

| **Zone III: Zone of Recurrent Ol + Cpx + Pl** |
| --- |

- Displays generally low values of Mg# and the highest levels of Ca, Al, alkalis and incompatible elements, including the rare-earth elements and high-field-strength elements;

- The chondrite-normalized spectra of incompatible elements are the most evolved;

- Involves the recurrent crystallization of olivine (Mg# 74.5–75.8) in association with relatively low-Mg Opx (Mg# 75.7–78.2);

- Appearance of primocrysts of Cpx (Mg# up to 88.0) and intercumulus Pl;

- Reaction rim of Prg at the interface of Cpx and Pl;

- Minor amounts of intercumulus Qz in veinlets; Qz is in a symplectitic intergrowth with Prg;

- Maximal enrichment of Cu in accessory base-metal sulfides.

| **Zone II: Zone of Dominant Orthopyroxene** |
| --- |

- Represents the major unit of the complex;

- Consists mainly of orthopyroxenite, in fine- to medium-grained variants, with a plane-parallel texture locally, or pegmatitic facies of Opx (up to 10–15 cm in size) developed typically close to contacts;

- The Opx tends to have its maximal degree of magnesium enrichment (Mg# up to 91–93) along the central axis of the complex;

- Grains of calcic Amp (Tr and Mhbl) are abundant and coexist with Opx, locally as a primary Amp and commonly as products of deuteric (autometamorphic) alteration.

| **Zone I: Olivine-Dominant Core-like Zone** |
| --- |

- Represents the earliest component of the complex;

- Includes the bulk of the Ol cumulates (in olivine orthopyroxenite, harzburgite and dunite) containing Ol with Mg# 89.1–90.3 in a centrally located large lens;

- Contains zones of chromitite.

Note. We have used the IMA-approved symbols [18]: Ol, olivine; Opx, orthopyroxene; Cpx, clinopyroxene; Pl, plagioclase; Amp, amphibole; Prg, pargasite; Mhbl, magnesio-hornblende; Tr, tremolite; Qz, quartz. The Mg# index is equal to $100 \, Mg/(Mg + Fe + Mn)$.

The first of these zones represents an exposed portion of a core of olivine-based cumulates, similar to the Central Dunite Zone of the zoned Chapesvara sill in the Serpentinite Belt [12]. The Lyavaraka complex differs from other members of the Serpentinite Belt (SB) in that the cumulates contain an unusually high proportion of orthopyroxene. This characteristic presumably reflects a higher level of silica in the melt, combined with essentially the same degree of magnesium enrichment, leading to hypermagnesian Opx with a Mg# of 91–93, among the highest in the Kola region. In addition, the Lyavaraka body is not a strikingly layered intrusive body, in spite of well-developed examples of planar features

observed locally in orthopyroxenite. We believe that Lyavaraka illustrates a "hybrid" form of organization, with characteristics of concentrically zoned complexes and some features of layered intrusions.

At an early stage, a central lens of Ol cumulates formed in Zone I, along with the associated Ol-bearing pyroxenite and zones of chromitites [20] (Figure 1b). Almost simultaneously with the early generation of Ol (Mg# 89.1–90.3), primocrysts of hypermagnesian Opx (Mg# 91–93) recorded in Zone II appeared on the liquidus in central portions of the crystallizing volume of melt, which could remain hotter longer. As another possibility, the hypermagnesian compositions of Opx may be a consequence of crystallization under conditions of elevated $fO_2$, as is the case for the chromian spinel in this complex [18]. This suggestion is consistent with the presence of notable (inferred) contents of ferric iron in such grains. For example, the representative composition (WDS) of orthopyroxene in sample LVR-3A is as follows: $SiO_2$ 57.83, $TiO_2$ 0.01, $Al_2O_3$ 0.05, $Cr_2O_3$ 0.02, FeO (total) 6.04, FeO (calc.) 4.58, $Fe_2O_3$ (calc.) 1.62, MnO 0.26, MgO 35.93, CaO 0.13, $Na_2O$ 0.02, $K_2O$ not detected (<0.01), Total 100.29 wt.%, which corresponds to the formula $(Mg_{1.83}Fe^{2+}_{0.13}Fe^{3+}_{0.04}Mn_{0.01}Ca_{0.01}Na_{<0.01})_{\Sigma 2.02}(Si_{1.98}Al_{<0.01})O_6$; the Mg# is 93.

In the Chapesvara complex, two generations of Opx were recorded: the first pertains to the original phase with a normal level of incorporation of Ca, Al and Cr. In contrast, grains of the second generation, formed by replacement of the original phase, are highly depleted in Ca, Al and Cr [12]. These observations agree with descriptions from the Pados-Tundra complex [6]. We can, therefore, presume that the hypermagnesian Opx compositions at Lyavaraka, which are also characteristically poor in Ca, Al and Cr, crystallized in a fluid-saturated magma with an elevated level of $fO_2$.

Most of the Opx cumulates of the complex formed at a second stage from the volume of derivative melt left after the Fo-rich Ol of Zone I had accumulated. It was likely saturated in $H_2O$ and still highly magnesian in composition even after the major event of Ol fractionation. The typical fine-grained orthopyroxenite, composed of the primary orthopyroxene–calcic amphibole association (Figure 8a), crystallized from portions of such a melt. In areas of high extents of accumulation of vapor and volatiles, pegmatitic megacrysts and huge spheroids of Opx formed (Figure 6a,b), as in the Pados-Tundra and Monchepluton complexes [8,55].

The final stage reflects the formation of the more evolved rocks of Zone III (Table 1) from the most fractionated melt positioned close to the boundary of the core-like zone (Figure 18). As noted, rocks and minerals of Zone III display a greater extent of magnesium depletion, with relatively higher levels of Ca, Al, alkalis, and incompatible elements. The configuration of this zone requires additional investigations; it may well be present in other areas close to or around the Ol-rich core, thus implying that this melt could be expelled, at least in part, during the crystallization of the core. As a consequence of the accumulated Ca and lower $MgO:SiO_2$ ratio (0.58–0.75; molar), the order of crystallization changed drastically. The primocrysts of magnesian Cpx, diopside with Mg# 87.4–88.0, crystallized first, and the less magnesian Opx grains (Mg# 78.4–81.5) appeared later.

Interestingly, small and irregular grains or patches of the second-generation olivine (Mg# 74.5–75.8) formed in association with Opx grains of relatively low-Mg compositions (Mg# 75.7–78.2). This later olivine is typically deposited along boundaries and after the grains of clinopyroxene (Figure 7b,c). We believe that these occurrences of Ol are additional consequences of a significant buildup in $fO_2$, which caused the appearance of an anomalous buildup of the geikielite component in ilmenite [18,19], owing to the conversion of $Fe^{2+}$ to $Fe^{3+}$ followed by a corresponding shortage in the content of ferrous iron. This shortage resulted in an increase in the Mg# in the fractionated melt.

The abundance of intercumulus Pl is noteworthy. It is virtually absent in the early formed zones of the complex, but formed in significant amounts in Zone III as a result of the buildup in Na, Ca and Al in the melt. A final event of mineral-forming processes is related to a further increase in the contents of volatiles ($H_2O$, $CO_2$, Cl, among others), which led to the formation of a reaction rim of pargasite at the boundary of grains of

Cpx and Pl (Figure 7d) and of grains of scapolite associated with Pl (Figure 8d). Minor amounts of intercumulus quartz, recorded in the form of deuteric veinlets or intergrown with pargasite (Figure 7d), are indicative of the extreme degree of magmatic differentiation in the Lyavaraka complex. This is the first reported example of modal quartz formed as a result of the fractional crystallization of an exceptionally high-Mg komatiitic parental melt in the Serpentinite Belt.

## 5. Conclusions

(1)   The Lyavaraka ultrabasic complex is one of several dunite–harzburgite–orthopyroxenite intrusive bodies that crystallized from an Al-undepleted komatiitic magma. They are exposed as shallow plutonic complexes in the Serpentinite Belt–Tulppio Belt (the SB–TB megastructure), which defines a large igneous province of Paleoproterozoic age.

(2)   The emplacement of the Lyavaraka and related complexes coincides with extension in the stable craton of the Fennoscandian Shield in the Early Paleoproterozoic. This geotectonic setting accounts for the shallow emplacement of highly magnesian komatiitic magma.

(3)   Zone I, an ultrabasic core-like zone, Zone II with predominant orthopyroxene, and Zone III, with recurrent Ol + Cpx + Pl, correspond to the three stages of crystallization of the Lyavaraka complex. Primocrysts of hypermagnesian Opx (Mg# 91–93) nucleated at a relatively high level of $fO_2$ in central areas of Zone II as olivine (Mg# 89.1–90.3) was forming in Zone I.

(4)   In Zone III, olivine grains of a second generation (Mg# 74.5–75.8) appeared after the primocrystic Cpx (Mg# up to 88.0). The recurrence of olivine is attributed to the progressive buildup in $fO_2$ and conversion of $Fe^{2+}$ to $Fe^{3+}$, well documented in earlier studies of oxide parageneses at Lyavaraka.

(5)   The elevated content of volatiles ($H_2O$, $CO_2$, Cl) in the highly magnesian magma accounts for its ability to be emplaced to a shallow crustal level. The occurrence of megaspheroids of orthopyroxene up to 12–15 cm across and of fine-grained orthopyroxene cocrystallized with Mg-rich calcic amphibole is indicative of a fluid-rich melt. Its degassing caused an increase in the intrinsic fugacity of oxygen.

## References

1. Shukevich, A.M. *An Account of Geological Mapping in the Rivers Nota and Pecha Basin in the Years 1932–1933 (Kola Peninsula)*; The Leningradsky (Northwestern) Geological Survey: Leningrad, Russia, 1933; Report in Russian.
2. Shukevich, A.M. *The Final Account of Field Investigations of the Pados-Tundra Geological Party No. 9 (Kola Peninsula)*; The Leningradsky (Northwestern) Geological Survey: Leningrad, Russia, 1936; Report in Russian.
3. Murashov, D.F. Ultrabasic intrusions of the Serpentinite Belt (Pados-Tundra and other). In *Geology of the USSR, Murmanskaya Oblast, Geological Description*; Gosgeoltekhizdat Publisher: Moscow, Russia, 1958; Volume 27, pp. 318–321. (In Russian)
4. Mamontov, V.P.; Dokuchaeva, V.S. The geology and ore potential of the Pados-Tundra massif in the Kola Peninsula. *Otech. Geol.* **2005**, *6*, 52–60. (In Russian)
5. Barkov, A.Y.; Nikiforov, A.A.; Barkova, L.P.; Korolyuk, V.N.; Martin, R.F. Zones of PGE–chromite mineralization in relation to crystallization of the Pados-Tundra ultramafic complex, Serpentinite Belt, Kola Peninsula, Russia. *Minerals* **2021**, *11*, 68. [CrossRef]
6. Barkov, A.Y.; Nikiforov, A.A.; Martin, R.F. The structure and cryptic layering of the Pados-Tundra ultramafic complex, Serpentinite Belt, Kola Peninsula, Russia. *Bull. Geol. Soc. Finl.* **2017**, *89*, 35–56. [CrossRef]
7. Barkov, A.Y.; Nikiforov, A.A.; Tolstykh, N.D.; Shvedov, G.I.; Korolyuk, V.N. Compounds of Ru–Se–S, alloys of Os–Ir, framboidal Ru nanophases, and laurite–clinochlore intergrowths in the Pados-Tundra complex, Kola Peninsula, Russia. *European J. Mineral.* **2017**, *29*, 613–621. [CrossRef]
8. Barkov, A.Y.; Nikiforov, A.A.; Halkoaho, T.A.A.; Konnunaho, J.P. The origin of spheroidal patterns of weathering in the Pados-Tundra mafic-ultramafic complex, Kola Peninsula, Russia. *Bull. Geol. Soc. Finl.* **2016**, *88*, 105–113. [CrossRef]
9. Barkov, A.Y.; Martin, R.F.; Izokh, A.E.; Nikiforov, A.A.; Korolyuk, V.N. Ultramagnesian olivine in the Monchepluton (Fo$_{96}$) and Pados-Tundra (Fo$_{93}$) layered intrusions (Kola Peninsula). *Russ. Geol. Geophys.* **2021**, *62*, 324–338. [CrossRef]
10. Serov, P.A.; Bayanova, T.B.; Steshenko, E.N.; Kunakkuzin, E.L.; Borisenko, E.S. Metallogenic setting and evolution of the Pados-Tundra Cr-bearing ultramafic complex, Kola Peninsula: Evidence from Sm–Nd and U–Pb isotopes. *Minerals* **2020**, *10*, 186. [CrossRef]
11. Vaasjoki, M. (Ed.) *Radiometric Age Determinations from Finnish Lapland and Their Bearing on the Timing of Precambrian Volcano-sedimentary Sequences*; Geological Survey of Finland: Espoo, Finland, 2001.
12. Barkov, A.Y.; Korolyuk, V.N.; Barkova, L.P.; Martin, R.F. Double-front crystallization in the Chapesvara ultramafic subvolcanic complex, Serpentinite Belt, Kola Peninsula, Russia. *Minerals* **2019**, *10*, 14. [CrossRef]
13. Barkov, A.Y.; Nikiforov, A.A.; Barkova, L.P.; Korolyuk, V.N. Komatiitic subvolcanic rocks in the Mount Khanlauta massif, Serpentinite Belt, Kola Peninsula. *Russ. Geol. Geoph.* **2022**, *63*, 1185–1207. (In Russian) [CrossRef]
14. Yang, S.H.; Hanski, E.; Li, C.; Maier, W.D.; Huhma, H.; Mokrushin, A.V.; Latypov, R.; Lahaye, Y.; O'Brien, H.; Qu, W.J. Mantle source of the 2.44–2.50-Ga mantle plume-related magmatism in the Fennoscandian Shield: Evidence from Os, Nd and Sr isotope compositions of the Monchepluton and Kemi intrusions. *Miner. Deposita* **2016**, *51*, 1055–1073. [CrossRef]
15. Melezhik, V.A.; Hanski, E.J. Palaeotectonic and palaeogeographic evolution of Fennoscandia in the Early Palaeoproterozoic. In *Reading the Archive of Earth's Oxygenation. 1*; The Palaeoproterozoic of Fennoscandia as Context for the Fennoscandian Arctic Russia—Drilling Early Earth Project; Melezhik, V.A., Prave, A.R., Fallick, A.E., Kump, L.R., Strauss, H., Lepland, A., Hanski, E.J., Eds.; Springer: Berlin/Heidelberg, Germany, 2013. [CrossRef]
16. Hanski, E.J. Evolution of the Palaeoproterozoic (2.50–1.95 Ga) non-orogenic magmatism in the eastern part of the Fennoscandian Shield. In *Reading the Archive of Earth's Oxygenation. 1*; The Palaeoproterozoic of Fennoscandia as Context for the Fennoscandian Arctic Russia—Drilling Early Earth, Project; Melezhik, V.A., Prave, A.R., Fallick, A.E., Kump, L.R., Strauss, H., Lepland, A., Hanski, E.J., Eds.; Springer: Berlin/Heidelberg, Germany, 2013. [CrossRef]
17. Kulikov, V.S.; Bychkova, Y.V.; Kulikova, V.V.; Ernst, R. The Vetreny Poyas (Windy Belt) subprovince or southeastern Fennoscandia: An essential component of the ca. 2.5–2.4 Ga Sumian large igneous provinces. *Precambrian Res.* **2010**, *183*, 589–601. [CrossRef]
18. Barkov, A.Y.; Nikiforov, A.A.; Korolyuk, V.N.; Barkova, L.P.; Martin, R.F. The chromian spinels of the Lyavaraka ultrabasic complex, Serpentinite Belt, Kola Peninsula, Russia: Patterns of zoning, hypermagnesian compositions, and early oxidation. *Can. Mineral.* **2021**, *59*, 1693–1709. [CrossRef]
19. Barkov, A.Y.; Nikiforov, A.A.; Korolyuk, V.N.; Barkova, L.P.; Martin, R.F. Anomalous chromite–ilmenite parageneses in the Chapesvara and Lyavaraka ultramafic complexes, Kola Peninsula, Russia. *Period. Mineral.* **2020**, *89*, 299–317. [CrossRef]
20. Spirov, V.N. Geological map (1:10 000) of the detailed mapping area at River Khlebnaya; an account of the western Kola geological party for the years 1968–1971. In *The Allarechensky Geological Party, North-Western Territorial Geological Department, Murmansk Geological-Prospecting Expedition*; The U.S.S.R. Ministry of Geology: Murmansk, Russia, 1972; Unpubl. Report in Russian.
21. Dokuchaeva, V.S. The geology and ore potential of the Mount Lyavaraka massif. In *Geology of Ore Deposits in the Kola Peninsula*; Kola Science Centre: Apatity, Russia, 1981; pp. 34–45. (In Russian)
22. Warr, L.N. IMA–CNMNC approved mineral symbols. *Mineral. Mag.* **2021**, *85*, 291–320. [CrossRef]
23. Korolyuk, V.N.; Usova, L.V.; Nigmatulina, E.N. Accuracy in the determination of the compositions of main rock-forming silicates and oxides on a JXA-8100 microanalyzer. *J. Anal. Chem.* **2009**, *64*, 1042–1046. [CrossRef]
24. Lavrent'ev, Y.G.; Korolyuk, V.N.; Usova, L.V.; Nigmatulina, E.N. Electron probe microanalysis of rock-forming minerals with a JXA-8100 electron probe microanalyzer. *Russ. Geol. Geoph.* **2015**, *56*, 1428–1436. [CrossRef]

25. Nikolaeva, I.V.; Palesskii, S.V.; Koz'menko, O.A.; Anoshin, G.N. Analysis of geologic reference materials for REE and HFSE by inductively coupled plasma-mass spectrometry (ICP-MS). *Geochem. Intern.* **2008**, *46*, 1016–1022. [CrossRef]
26. Nikolaeva, I.V.; Palesskii, S.V.; Chirko, O.S.; Chernonozhkin, S.M. Determination of major and trace elements by inductively coupled mass-spectrometry in silicate rocks after fusion with $LiBO_2$. *Anal. I Control* **2012**, *8*, 134–142.
27. Karmanova, N.G.; Karmanov, N.S. A universal methodology of X-ray fluorescence analysis of rocks using an ARL-9900XP spectrometer. In Proceedings of the VII All-Russian Conference on X-ray Spectral Analysis, Novosibirsk, Russia, 19–23 September 2011; p. 126. (In Russian).
28. Balagansky, V.V.; Gorbunov, I.A.; Mudruk, S.V. Palaeoproterozoic Lapland-Kola and Svecofennian Orogens (Baltic Shield). *Her. Kola Sci. Cent. RAS* **2016**, *3*, 5–11. (In Russian)
29. Balagansky, V.V.; Glebovitsky, V.A. The Lapland granulite belt and the Tanaelv belt. In *Early Precambrian of the Baltic Shield*; Nauka: Saint-Petersburg, Russia, 2005; pp. 127–175. (In Russian)
30. Mindlina, A.A. Geological Map of the USSR, scale 1:200,000, the Kola Series (R-35-XXXV, XXXVI). In *North-Western Geological Department, 1958*; Shukevich, A.M., Ed.; Ministry of Geology and Mineral Resources Protection, Gosgeoltekhizdat Publisher: Moscow, Russia, 1959.
31. Belyaev, K.D. Geological Map of the USSR, scale 1:200,000, the Kola Series (R-36 XXXI, XXXII). In *North-Western Geological Department, 1960*; Polferov, D.V., Ed.; Ministry of Geology and Mineral Resources Protection, Gosgeoltekhizdat Publisher: Moscow, Russia, 1962.
32. Lunina, O.P.; Roginskaya, B.I. Geological Map of the USSR, scale 1:200,000, the Kola Series (Q-36-I). In *North-Western Geological Department, 1960*; Shurkin, K.A., Ed.; Ministry of Geology and Mineral Resources Protection, Gosgeoltekhizdat Publisher: Moscow, Russia, 1962.
33. Solodkaya, R.I. Geological Map of the USSR, scale 1:200,000, the Kola Series (Q-36-II). In *North-Western Geological Department, 1961*; Perevozchikova, V.A., Ed.; Ministry of Geology and Mineral Resources Protection, Gosgeoltekhizdat Publisher: Moscow, Russia, 1963.
34. Leontyeva, O.P.; Belonin, M.D. Geological Map of the USSR, scale 1:200,000, the Kola Series (Q-35-VI). In *North-Western Geological Department, 1961*; Shurkin, K.A., Ed.; Ministry of Geology and Mineral Resources Protection, Gosgeoltekhizdat Publisher: Moscow, Russia, 1964.
35. Lindh, A.; Eskelinen, J.; Luukas, J.; Kousa, J.; Nironen, M. *The Bedrock of Finland 1:200,000 Map Modified from the General Map 1:1 Million*; National Land Survey of Finland, Geological Survey of Finland: Espoo, Finland, 2014.
36. Nironen, M.; Kousa, J.; Luukas, J.; Lahtinen, R. (Eds.) *Geological Map of Finland—Bedrock 1:1,000,000*, 2nd ed.; Geological Survey of Finland: Espoo, Finland, 2016.
37. Morimoto, N. Nomenclature of pyroxenes. *Can. Mineral.* **1989**, *27*, 143–156. [CrossRef]
38. Schmid-Beurmann, P.; Bente, K. Stability properties of the $CuS_2$-$FeS_2$ solid solution series of pyrite type. *Mineral. Petrol.* **1995**, *53*, 333–341. [CrossRef]
39. Grove, T.L.; Parman, S.W. Thermal evolution of the Earth as recorded by komatiites. *Earth Planet. Sci. Lett.* **2004**, *219*, 173–187. [CrossRef]
40. Robin-Popieul, C.C.M.; Arndt, N.T.; Chauvel, C.; Byerly, G.R.; Sobolev, A.V.; Wilson, A. A new model for Barberton komatiites: Deep critical melting with high melt retention. *J. Petrol.* **2012**, *53*, 2191–2229. [CrossRef]
41. McDonough, W.F.; Sun, S.-S. The composition of the Earth. *Chem. Geol.* **1995**, *120*, 223–253. [CrossRef]
42. Vinogradov, L.A. Formations of Alpine-type ultrabasic rocks in the southwestern part of the Kola Peninsula (The Notozerskiy ultrabasic belt). In *Problems of Magmatism of the Baltic Shield*; Nauka Publisher: Leningrad, Russia, 1971; pp. 147–153. (In Russian)
43. Puchtel, I.S.; Haase, K.M.; Hofmann, A.W.; Chauvel, C.; Kulikov, V.S.; Garbe-Schönberg, C.-D.; Nemchin, A.A. Petrology and geochemistry of crustally contaminated komatiitic basalts from the Vetreny Belt, southeastern Baltic Shield: Evidence for an early Proterozoic mantle plume beneath rifted Archean continental lithosphere. *Geochim. Cosmochim. Acta* **1997**, *61*, 1205–1222. [CrossRef]
44. Alapieti, T.; Filen, B.; Lahtinen, J.; Lavrov, M.; Smolkin, V.; Voitsekhovsky, S. Early Proterozoic layered intrusions in the northeastern part of the Fennoscandian Shield. *Mineral. Petrol.* **1990**, *42*, 1–22. [CrossRef]
45. Amelin, Y.V.; Heaman, L.M.; Semenov, V.S. U–Pb geochronology of layered mafic intrusions in the eastern Baltic Shield: Implications for the timing and duration of Paleoproterozoic continental rifting. *Precamb. Res.* **1995**, *75*, 31–46. [CrossRef]
46. Barnes, S.J.; Fiorentini, M.L. Komatiite magmas and sulfide nickel deposits: A comparison of variably enriched Archean terranes. *Econ. Geol.* **2012**, *107*, 755–780. [CrossRef]
47. Barkov, A.Y.; Nikiforov, A.A.; Barkova, L.P.; Martin, R.F. Occurrences of Pd–Pt bismuthotellurides and a phosphohedyphane-like phase in sulfide veins of the Monchepluton layered complex, Kola Peninsula, Russia. *Minerals* **2022**, *12*, 624. [CrossRef]
48. Stone, W.E.; Deloule, E.; Larson, M.S.; Lesher, C.M. Evidence for hydrous high-MgO melts in the Precambrian. *Geology* **1997**, *25*, 143. [CrossRef]
49. Wilson, A.H.; Shirey, S.B.; Carlson, R.W. Archaean ultra-depleted komatiites formed by hydrous melting of cratonic mantle. *Nature* **2003**, *423*, 858–861. [CrossRef] [PubMed]
50. Czamanske, G.K.; Wones, D.R. Oxidation during magmatic differentiation, Finnmarka complex, Oslo area, Norway. 2. The mafic silicates. *J. Petrol.* **1973**, *14*, 349–380. [CrossRef]
51. Arndt, N.T. Thick, layered peridotite–gabbro lava flows in Munro Township, Ontario. *Can. J. Earth Sci.* **1977**, *14*, 2620–2637. [CrossRef]
52. Arndt, N.T. Differentiation of komatiite flows. *J. Petrol.* **1986**, *27*, 279–301. [CrossRef]

53. Nesbitt, R.W.; Jahn, B.-M.; Purvis, A.C. Komatiites: An early Precambrian phenomenon. *J. Volcanol. Geotherm. Res.* **1982**, *14*, 31–45. [CrossRef]
54. Hanski, E.; Huhma, H.; Rastas, P.; Kamenetsky, V.S. The Palaeoproterozoic komatiite–picrite association of Finnish Lapland. *J. Petrol.* **2001**, *42*, 855–876. [CrossRef]
55. Barkov, A.Y.; Nikiforov, A.A.; Martin, R.F. A novel mechanism of spheroidal weathering: A case study from the Monchepluton layered complex, Kola Peninsula, Russia. *Bull. Geol. Soc. Finl.* **2015**, *87*, 79–85. [CrossRef]